ELSEVIER

Journal of Molecular Structure (Theochem) 675 (2004) 95–105

THEO CHEM

www.elsevier.com/locate/theochem

Structure, spectra and the effects of twisting of β-sheet peptides. A density functional theory study

Petr Bour[a,1], Timothy A. Keiderling[b,*]

[a]*Institute of Organic Chemistry and Biochemistry, Academy of Sciences of the Czech Republic, Flemingovo nám. 2, 16610, Praha 6, Czech Republic*

[b]*Department of Chemistry, University of Illinois at Chicago, 845 W. Taylor Street (M/C 111), Chicago, IL 60607-7061, USA*

Abstract

The structure, infrared (IR) absorption and vibrational circular dichroism (VCD) spectra and their response to twisting of a model peptide dimer $(Ac-Ala_3-NHMe)_2$ in vacuum is calculated with density functional theory (DFT) methods at the BPW91/6-31G** level and compared in terms of twisting energetics to HF and MM level results. The differences in spectral frequencies and IR and VCD intensity distributions for fully relaxed parallel and anti-parallel β-sheet arrangements, as well as for sheets with constrained twist are discussed and contrasted with known experimental data. Due to the hydrogen bonds between the strands, short (4 amide) strands assembled into β-sheets were found to be stable in vacuum with DFT, unlike the case for helical conformations. For these optimized β-structures, calculated IR spectra for parallel and anti-parallel alignments are distinguishable for the minimum energy structures and respond differently to twist distortion. The associated VCD intensity patterns reflect the sense of the sheet twists and are also predicted to discriminate between parallel and anti-parallel forms.

Keywords: Ab initio optimized geometry; Peptide secondary structure; Conformation; Infrared absorption; Vibrational circular dichroism

1. Introduction

Peptide structure has long been modeled using classical (molecular mechanics, MM) methods. Similarly peptide vibrational spectra have been computed using empirical force fields (FF) that were optimized to fit experimental data [1]. Only recently have computational facilities and available software been capable of optimizing geometries and computing energies at an ab initio quantum mechanical level for peptides of a size to allow sensible comparison to experimental structures of molecules of biological relevance. The situation for simulation of spectral properties has lagged further. Electronic spectra (uv absorption, fluorescence, circular dichroism) require excited state calculations, and thus demand considerable approximation and are limited to relatively small molecules if meaningful quantum mechanical results are required. For vibrational spectra, only second derivatives of the energy are required to obtain a FF and hence frequencies. For infrared (IR) and vibrational circular dichroism (VCD) spectral simulations, dipole derivatives (atomic polar (APT) and axial (AAT) tensors) and, for Raman, polarizability derivatives must be computed. For VCD, these are typically obtained using a ground-state formalism based on the magnetic field perturbation (MFP) theory of Stephens, implemented at the harmonic approximation within density functional theory (DFT) methods [2,3]. The DFT implementation of MFP theory utilizing gauge-independent atomic orbitals (GIAO) has been especially successful [4–8]. While computation of structures is an obviously valuable application of DFT techniques, the extension of quantum chemical methods to simulation of vibrational spectra provides a means of testing the relevance of these structural calculations against readily available experimental data that are structurally sensitive. This was shown by us and others who have employed DFT spectral simulations to probe structural properties of a variety of peptides [9–18].

Several studies [14–22] have focused on small peptides (partially due to their imposing less calculational constraints with fewer atoms) exploring intrinsic conformations and effect of solvent and other perturbations. Larger peptide studies have mostly emphasized helical conformations since

* Corresponding author. Tel.: 312-996-3156; fax: 312-996-0431.
E-mail addresses: tak@uic.edu (T.A. Keiderling), bour@uochb.cas.cz (P. Bour).
[1] Fax: 420-224-310-503.

0166-1280/$ - see front matter © 2004 Elsevier B.V. All rights reserved.
doi:10.1016/j.theochem.2003.12.046

such structures form the dominant uniform (or extended) secondary structural element in proteins. We have shown that spectra can be simulated for α-helical peptides (up to a decapeptide) that match IR and VCD results on a semiquantitative level (~5% frequency error, ~20% IR intensity error, plus reproduction of signs and relative intensities of most VCD bands) [9,10,12,19]. To carry out these calculations, the structures were fully optimized with the exception that the ϕ, ψ angles were constrained to yield the helical conformation desired. Even larger peptide spectra can be simulated by transfer of spectral parameters obtained from these model DFT computations onto larger structures [12,23]. Spectral differentiation of α-helices from other helical structures, with most emphasis on the left-handed 3_1-helix (or P_{II}) that is found in poly-L-proline II, collagen and (most probably) in denatured proteins and random coil peptides [24], and the 3_{10}-helix (right-handed, $i \rightarrow i+3$ hydrogen bonds), which may be an intermediate in helix folding processes [25], was shown to be possible if peptides were constrained to those structures for simulation and if IR and VCD analyses were combined [9,11–13]. However, only the 3_{10}-helix was found to be stable in vacuum (no solvent) DFT calculations for peptides increasing in length up to structures containing ten amide bonds [10]. Thus, though calculational studies including spectral simulations on constrained helices are plentiful, such computations with full structural optimizations are limited.

Our approach to the study of β-sheets initially used this same torsional constraint concept [26–28]. Those studies demonstrated that the characteristic amide I (C=O stretch) IR absorption, an intense, sharp band between 1630–1610 cm^{-1} with a weak component at 1680–90 cm^{-1} was sensitive in terms of frequency splitting (exciton width) and intensity distribution to the number and length of the strands as well as the overall flatness of the sheet. The more the sheet twisted with a right-handed sense, such as is universally found in protein structures, the splitting became less and the spectra became broader. Parallel structures also showed less splitting than anti-parallel, suggesting a potential means of discriminating between them. Amide I VCD spectra for twisted sheets were predicted to be decidedly more intense than for planar sheets, which does agree with the relative VCD intensities for β-sheet proteins as compared to extended flat sheets in aggregated polypeptides [29–34]. However, the overall patterns, while varying between structural types and again distinctive between the specific twisted parallel and anti-parallel structures that were modeled, were not definitive since the predicted VCD intensities were low and sensitive to the detailed geometry and since few experimental spectra were known for pure β-sheets to allow useful tests of the validity of the theoretical results. The latter situation is now changing due to the development of a number of viable model β-hairpin peptides some of whose structures are also being determined using nmr tools [35–39]. Hairpins, in particular, often have a significant degree of twist so that new model calculations systematically accounting for this property are needed. Furthermore, the effect of constraining the structure to model β-sheet ϕ, ψ torsional angles has not been explored.

In this paper we compute fully relaxed geometries and IR and VCD spectra for a set of dimers of tetra amide strands, $(Ac-Ala_3-NHCH_3)_2$, containing both parallel and anti-parallel conformations. In addition, by use of our normal mode-based optimization method [40], modified for constrained strand twist, we explore the effect on spectra of twisting the resultant 2-stranded sheet. Most of our analyses focus on the amide I, since the amide II and other modes are more affected by solvation and H-bonding to the solvent. These lower frequency modes are also much less simple to study with IR and VCD than the amide I. However the amide III in combination with the Cα–H deformations may prove useful for such conformational discriminations using UV resonant Raman [21,41–44] or Raman optical activity techniques [45]. Such solvent effects and consequences of expanding the sheet in both length and number of strands will be explored separately in a subsequent publication [46]. We have established that H-bonds to the peptide and compensation for solvent effects are major factors in the normal frequency error found especially in DFT FF calculations of amide I spectra [15,16,22,47]. Nonetheless our model calculations indicate that these solvent effects primarily shift frequencies and do not substantially alter bandshapes and relative intensities. Thus DFT calculations of the vibrational properties of peptides in vacuum can be used to simulate qualitative spectral patterns and establish relative spectral changes between various structural types and determine their sensitivity to model constraints. The latter diagnostic is the type of information sought in this paper.

2. Method

The $(Ac-Ala_3-NHMe)_2$ dimer was chosen as a test case, in part due to our computer limitations, since it allowed us to perform these computations at fully ab initio DFT level with our usual degree of precision. Choosing an even number of amide groups in both strands can balance the hydrogen bonding that stabilizes the sheet so that neither end is favored. Additionally, for the anti-parallel structure calculations, the C_2 symmetry was used to save computation time.

The dimer geometry optimizations were initially started from idealized parallel and two anti-parallel conformations (API and APII) that differ in the positioning of the H-bonds coupling the two strands. In each case, the geometry was fully optimized in vacuum at the BPW91/6-31G** level, which was previously found to be an optimal level for simulation of amide spectra for larger peptides [11]. All DFT calculations used the Gaussian98 program package [48].

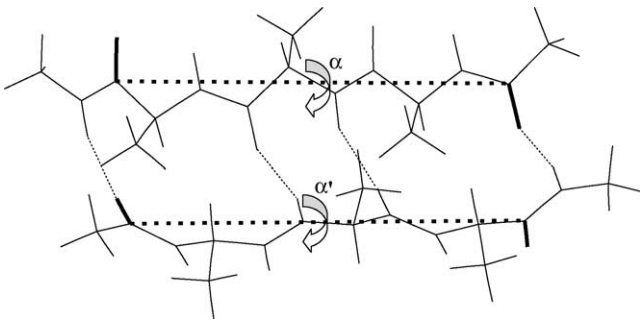

Fig. 1. Definition of the two O=C···C=O (shown in bold) strand torsion angles, α, α', used for controlling the sheet twist (example shown is for the API anti-parallel structure, where $\alpha = \alpha'$).

In addition to the unconstrained DFT geometry optimizations, various degrees of twist, such as might be caused by external forces, were imposed on the pairs of peptide strands. Restricted optimizations of the geometry were computed, for which the torsion angles (α, α' as defined in Fig. 1) between the terminal carbonyl groups were kept at a series of constant values. The usual algorithms for this purpose, based on the redundant internal coordinates [49], are notorious for performing badly on systems containing hydrogen bonds, such as our dimer of oligopeptides. This leads to numerical instabilities, resulting in poor or, in many cases, no convergence. Fortunately, we found that the more stable (although generally slower) normal mode optimization method [40] can be modified and used in place of the more commonly employed redundant coordinate method implemented in Gaussian98. The geometry restrictions were implemented as additional FF terms. For example, in order to fix the strand torsion angle (Fig. 1), a harmonic term ($\sim (\alpha - \alpha_0)^2$) was added to the molecular energy in our external normal coordinate program, *qgrad*, and the normal mode optimization method was used as previously described [40]. (Fixing normal modes, the primary purpose of the *qgrad* program, was not used in this application.) Additionally, SCF computations at the HF/4-31G level and MM computations, the latter with the Tinker program [50] and Amber FF, were used for comparative computations of twisting energetics as indicated in the relevant section below.

For the optimized geometries, harmonic FF (FF) and atomic polar (APT) and atomic axial (AAT) tensors were calculated at the same (BPW91/6-31G**) level also by means of GAUSSIAN98. It might be noted that we have found that this level of DFT yields very good amide I and II spectral results for a number of structures and is much more efficient for FF computation than the hybrid functionals (e.g. B3LYP) commonly used for vibrational analyses. This advantage may result from our focus on a few characteristic amide bands and our avoidance of aromatic components and that part of the spectrum at lower frequencies, which involves modes of a more mixed character. We have not tested this latter hypothesis in detail. However, the 'pure' BPW91 functional has also performed better for other systems, such as polycyclic hydrocarbons and DNA components [51–53]. The APT and AAT values are required, along with the normal modes, for computation of the VCD and IR spectra through use of the DFT-GIAO based MFP theory [4,8]. Realistic spectra were simulated with in-house programs by positioning Lorentzian bands with a width of 15 cm^{-1} FWHM on each transition, to match the experimental resolution, and with IR and VCD intensities scaled to the dipolar and rotational strengths, respectively.

3. Results

3.1. Fully optimized structure calculations

The parallel and both anti-parallel β-sheet structures were found to be stable in vacuum at the BPW91/6-31G** level. The equilibrium geometries determined are shown in Fig. 2. This convergence is in contrast to our previous experience with decapeptide helices, for which only the 3_{10}-helix structure was maintained as a stable conformation in vacuum [10]. It is worth noting, particularly in the parallel case, that the β-structure is partially stabilized by

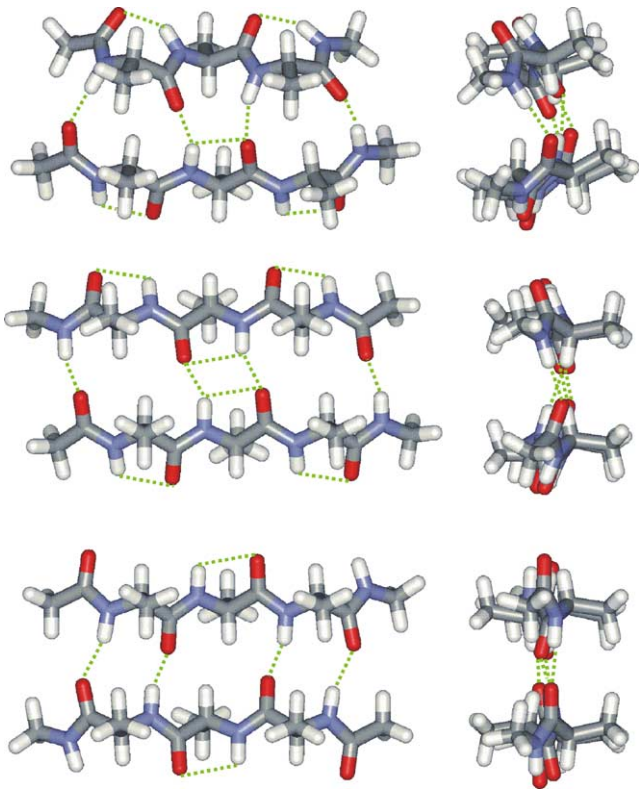

Fig. 2. Optimized (BPW91/6-31G**) parallel (P, top), and anti-parallel (API, middle, and APII, bottom) β-sheet structures, shown from the side (left) and end (right) of the two-stranded structures. Hydrogen bonds are emphasized by the dashed lines.

Table 1
Energies and dipole moments of the fully optimized β-structures

Conformation	Energy (Hartree)	Relative energy (kcal/mole)	Dipole moment (Debye)
Parallel (P)	−1980.896237	0.90	1.00
Anti-parallel I (API)	−1980.897671	0	0.71
Anti-parallel II (APII)	−1980.882195	9.71	0.42

hydrogen bonds between the N–H and C=O groups on the outer edges, which then form 5-member rings, although these bonds are longer (~2.2–2.3 Å) than the inter-strand H-bonds (1.9–2.1 Å). These outer edge H-bonds can also help explain the relatively large energy difference between the two anti-parallel forms (Table 1), since the API and APII forms can form two and four such H-bonded rings, respectively. However, in aqueous solvent such a minor advantage would be significantly modified. The difference between the energies of the P and API dimers (Table 1) is small, and without consideration of solvent and other effects one cannot say if such a small bias favorable to the anti-parallel form could explain its more common occurrence in natural structures. That bias may just result from the ease of aligning anti-parallel strands interspersed with a loop or turn structure.

In order to find out how closely our model calculations approach the structures of real systems, in Table 2 we compare the chain torsion angles and hydrogen bond lengths of these computed dimers to experimental values obtained for selected 'typical' β-sheet proteins. Note, that the number of independent parameters is reduced for API and APII, due to the C_2 symmetry that was used to improve computational efficiency. Both the angles and the hydrogen bond lengths can be viewed as agreeing with the experimental numbers, perhaps with the exception of the parallel sheet, where a bigger dispersion was calculated for the (φ, ψ) angles. However, the experimental ranges are large, which suggests that as being a source of the general problems in characterizing β-sheets with spectroscopic probes that are sensitive to variation in stereochemical parameters. The computed non-planarity of the amide group, measured by the ω angle, also falls within the dispersion found in X-ray structures of proteins [54] where the non-planarity is correlated with the experimental (φ, ψ) values. Since our computations are restricted to only one system, no definite conclusions in the latter regard can be made in this point. The twist calculated for the equilibrium structures is relatively small, being $(\alpha, \alpha') = (-172.7, -173.5°)$ for the parallel, and −177.4 and −169.3° for the API and APII models (where $\alpha = \alpha'$), respectively.

3.2. Twisted structure calculations

Detailed structural characteristics of natural β-sheets depend on various factors including hydrogen bonding, hydrophobic interactions, specific side-chain binding and sequence of the peptide chain. In order to determine the energetics and spectral properties of our model with respect to the sheet twist, the angles α, α' were varied. For API the dependencies of the relative energies on the twist, as calculated at the BPW91/6-31G**, HF/4-31G and MM/Amber levels, are compared in Fig. 3. The first two (presumably more accurate) levels predict a minimum energy close to $\alpha, \alpha' = 180°$, with distortions of the surfaces that slightly favor conformations with negative α. The Amber FF

Table 2
Torsion angles and hydrogen bond lengths in the β-sheet structures

Conformation I. Calculated values[a]	ω	φ	ψ	d(O··H)
P	−177.8, −171.8, −176.3, −176.4, 177.2, 175.1, 171.1, 177.2	−82.7, −98.6, −82.4, −147.7, −155.1, −133.0	78.3, 90.0, 75.0, 153.6, 165.4, 143.4	1.92, 1.97, 2.12, 1.95
AP I	177.6, 171.4, 176.7, 176.5	−140.9, −156.0, −149.3	150.2, 154.6, 153.2	1.93, 2.08
AP II	178.3, 173.6, 176.8, 180.0	−121.5, −138.1, −132.0	143.7, 141.6, 119.8	2.12, 1.89
II. Structural parameters in natural proteins[a]				
Parallel:				
Pectase lyase C segments[b]	−179–176	−111– −135	102–145	1.89–2.29
Anti-parallel:				
poly-L-Ala (almost planar)[c]	−178.5	−138.6	134.5	1.90
Intestinal fatty acid binding protein-segment (twisted)[d]	−173–171	−105– −149	120–153	1.81–2.15
BPTI segments (super-coil)[e]	180	−114/−92	150/114	1.84

Values represent 'Top' and 'bottom' peptide chain, from left to right in Fig. 2.
[a] (ω, φ, ψ), in degrees, (d) in Å.
[b] PDB code: 2PEC, (X-ray), Ref. [59].
[c] (X-ray), Ref. [71].
[d] PDB code: 1IFC, (X-ray), Ref. [72].
[e] Bovine pancreatic trypsin inhibitor (BPTI), Ref. [55].

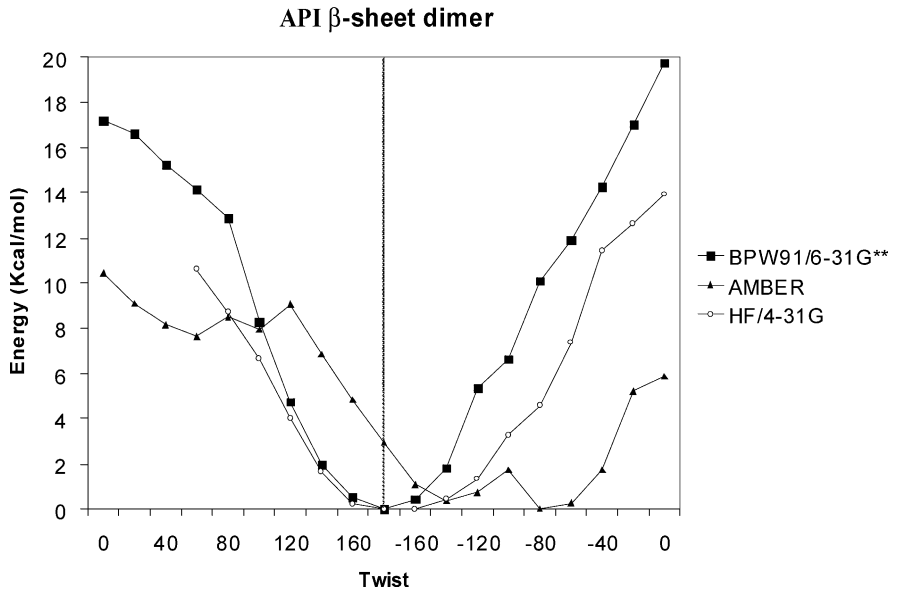

Fig. 3. The dependence of the calculated relative energy on the twist of the peptide chain (expressed as α, see Fig. 1) for the API structure (see Fig. 2, middle) calculated at three levels of approximation, DFT/BPW91/6-31G** (solid squares), SCF.HF/4-31G (open circles) and MM/Amber (solid trangles).

resulted in minima at $\alpha, \alpha' = -140$ and $-80°$, much more biased to the right-handed sheet twist. At room temperature ($kT \sim 0.6$ kcal/mol) one may expect that the sheet can twist almost freely between $+160$ and $-160°$, from both the DFT and HF results, an interval of approximately 40, or $\sim 13°$ per amino acid. More twisted structures may of course be stabilized for a realistic β-sheet by its environment, including hydrogen bonding or hydrophobic interactions in proteins. This is consistent with the calculations predicting that even larger twisting angles (e.g. from $+80$ to $-80°$) are accessible with relatively low added energy penalties, of the order of ~ 2 kcal/mol per amino acid residue.

At the BPW91/6-31G** level, similar dependencies for peptide energies on the twist angle were calculated for the *P* and APII models as plotted in Fig. 4. Although we investigated a physically unreasonable range of these α, α' angles for API, we consider the energies obtained for twists significantly deviated from 180° to be unreliable, since then the sheet becomes severely distorted and ill-defined. For very high twists, the strands fail to stay aligned [55]. Qualitatively, the dependence in Fig. 4 is similar for all the *P*, API and APII forms: the equilibrium structure is almost planar ($\alpha \sim 180°$) and the shallow minimum suggests that the β-sheet structure is to some extent susceptible to

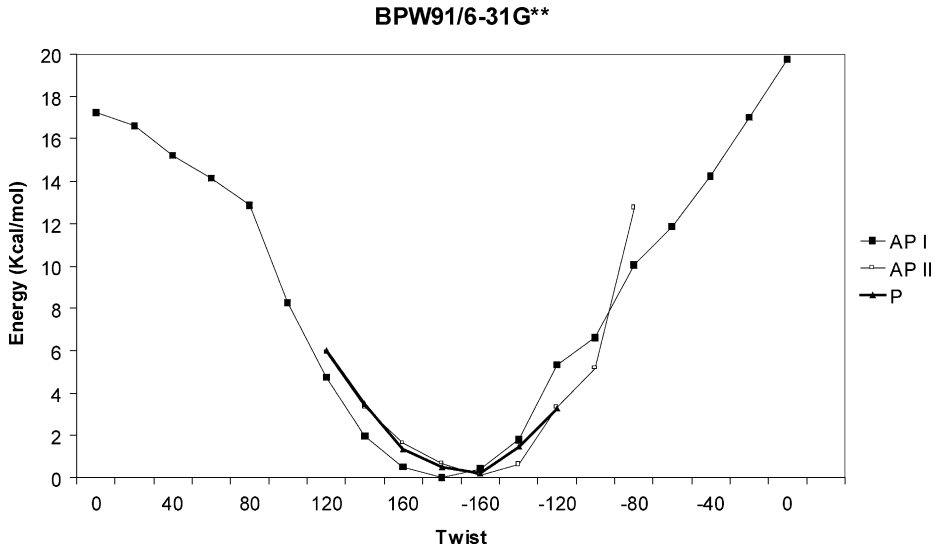

Fig. 4. The dependence of the relative DFT energy on the twist, α, for the three types of the β-sheet studied, API (solid squares), APII (open circles) and P (solid trangles), as calculated for the dimer at the BPW91/6-31G** level.

external perturbations. The APII and P forms have their minima shifted towards −160° and overall are asymmetrically distributed favoring the right-hand twist conformation.

3.3. Basic spectral characteristics

Absorption and VCD spectra of the equilibrium structures are plotted in Fig. 5, for the two anti-parallel and the parallel forms. Spectra of both the protonated (solid line) and N-deuterated (dashed line) molecules were simulated to account for experiments on samples in both H_2O and D_2O solvents. The predicted spectra in general agree with previous simulations for constrained β-sheets, but detailed assignment of their vibrational modes will differ somewhat since the CH_3 mode overlap was not removed here (in the region $\sim 1450\ cm^{-1}$) as was done in our previous β-sheet simulations [26,27]. The principal spectral difference between these fully relaxed tetrapeptide-based parallel and anti-parallel forms and the previous constrained, tripeptide-based results stems from the nature of the amide I splitting for the two forms. Both anti-parallel cases have $\sim 35\ cm^{-1}$ splitting with a lower frequency component being much more intense, yielding the characteristic β-sheet type amide I IR absorption. The frequencies are about $50\ cm^{-1}$ higher than found experimentally, as expected for DFT calculations without solvent correction [22]. Due to end effects, there are actually weak modes lower in frequency than the dominant intense one, which tends to involve stretches of the central C=O groups in both API and APII. The parallel case has a different intensity distribution, with several components being intense, distributing dipole strength across the band. This deviates from previous simulations for flat sheets but partially reflects results from twisted parallel sheets [26]. This can result in the higher frequencies found experimentally for twisted parallel sheets in protein samples.

In the API and APII absorption spectra, the unbound (or weakly interacting) carbonyl groups contribute most to the high frequencies 1700–1720 cm^{-1}, while the cross-strand interior H-bonded carbonyls contribute more to the dominant absorption maximum at low frequency (here calculated to be $\sim 1675\ cm^{-1}$), whose intensity is 2–3 times higher. This partitioning to different C=O types is emphasized by the short strand length and would become less localized in a multi strand amide. (Exciton coupling would develop a delocalized normal mode with most of the intensity [56].) For the parallel sheet, the stretching modes from the carbonyl groups are more mixed, which leads to their forming a broader absorption maximum which is higher in frequency than the anti-parallel cases. This pattern

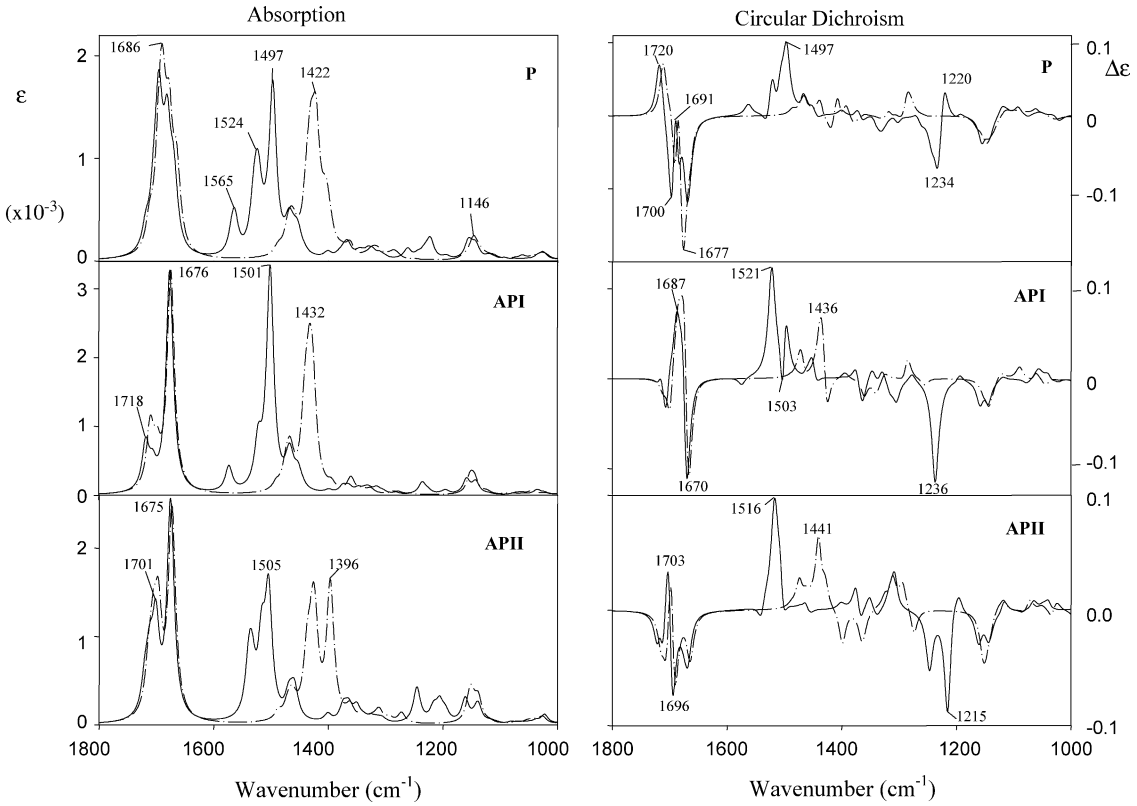

Fig. 5. IR Absorption and vibrational circular dichroism as calculated for the parallel (P) and two anti-parallel (API and APII) β-sheet models, comparing N–H (solid lines) with N-D exchanged (dashed lines) simulated spectra for much of the mid-IR range.

is virtually unperturbed and only slightly shifted by deuteration.

The high intensity of the amide II seems to be a result of having just two strands, since previous multi-strand simulations lead to intensities more in agreement with experiment [26]. The multiple components of the amide II are also an effect of the calculation being done in vacuum. The edge N–Hs (not hydrogen bonded) will have lower amide II frequencies and higher intensities. These spectral variations also reflect differences in structure: for the parallel case (*P*) the outer N–H and C=O groups form shorter (~2 Å) edge hydrogen bonds than in the API and APII anti-parallel dimers (where the distance between the acidic hydrogen and oxygen is around 2.3 Å).

The spectral difference between conformations is less pronounced in the amide II vibrational region. For AP I and II, the highest intensity corresponds to amide groups with weakly bond hydrogen atoms (NH groups pointing outwards), while the amide groups with hydrogens participating in inter-strand binding provide weaker amide II transitions at higher frequencies. For the parallel form, the amide II frequencies are less separated with the most intensity at low frequencies. For the deuterated forms the amide II signal is more complex due to the coupling to other (side-chain) modes.

Parallel and anti-parallel sheets can also be distinguished on the basis of VCD spectra, at least for these fully minimized tetrapeptide-based models. While both forms have negative VCD for the lower frequency amide I components, the anti-parallel form exhibits an ambiguous sign for the high frequency exciton component while the parallel structure has a positive VCD in this region. Similarly, between the extremes, the net VCD signals of the parallel and anti-parallel structures are predicted to be negative and positive, respectively. In the amide II region (~1490–1550 cm^{-1}) both forms give a net positive signal. Also the amide III frequency region (computed around 1220 cm^{-1}) reflects the difference between parallel (conservative VCD couplet) and anti-parallel (negative VCD) sheets. Based on our previous experience, we may expect a shift in absolute values of frequencies for experimental spectra, caused by solvent effects, anharmonic interactions and computational error. However, the relative frequencies and the VCD sign pattern should not be influenced by these factors.

3.4. Twist distortion and effect on spectral pattern

The absorption spectra are relatively resistant to the β-sheet twist, the lower frequency modes are essentially unchanged, with only the amide I providing much twist sensitivity in the IR. For example, the parallel conformer IR spectra change primarily in magnitude of the amide I component bands over a variation of $\alpha = 120- - 120°$ (through 180°) as seen in Fig. 6a for the overlapped spectra of six twisted dimers of the parallel (*P*) sheet. However, for the API case (Fig. 6b), the main amide I feature shifts up in frequency at negative α, due to a reduction in splitting of the band, since the high frequency component is stable. The main dipole intensity remains in the low frequency modes.

This dependence on twist is summarized in Table 3, where the predicted frequencies of the amide I and amide II absorption maxima are tabulated for the P, API and APII conformers as a function of twist, α. For the parallel form the frequencies of the amide I components are almost unaffected by the twist (variance of 4–6 cm^{-1}), but their intensities change markedly. By contrast, the amide I frequencies of the two anti-parallel structures change more, suggesting the possibility of correlating the maximum frequency and the twisting angle, but the relative intensities are more stable. This difference in parallel and anti-parallel overall intensity maxima occurs because the amide I splitting is reduced by the twist angle and the anti-parallel absorption maximum corresponds to one of the lower frequency components of the split band. On the contrary, since the parallel maximum is in the center of the band its position is less sensitive to the twist effects on its width.

The twist does cause important changes in the VCD intensities. In Fig. 7 the dependence of the simulated amide I′ (N-deuterated, to correspond with the modes most often measured for sheet peptides) VCD spectra of the P, API and APII dimers is shown. In this variation, VCD patterns are seen to change sign as α varies from the positive to negative side (left- to right-hand twist) confirming that the VCD originates in C=O coupling, dipolar or mechanical, between residues. On the other hand, the amide II and III (N-protonated) variances with α are much less for a given conformational type (data not shown). The parallel sheet (*P*) twist variations result in dominantly negative amide I signals, but these are composed of successive negative couplets (− then + with increasing frequency) that shift in intensity distribution as α becomes negative. For the API form, twist with positive α leads to a VCD intensity increase in the amide I region, where the signal approaches a conservative negative couplet pattern centered on the intense low frequency IR component, while negative α leads to a weaker but positive couplet VCD for this transition. The APII form has a bigger dispersion of the amide I VCD intensity and less intensity differentiation between the high and low components, which appear to be oppositely signed couplets that change sign with change of sign of α, but overall maintain a qualitatively similar (mirror image) VCD pattern. Importantly, the bias, or net VCD (if resolution were reduced), of both anti-parallel forms, API and APII, changes from positive ($\alpha > 0$) to negative ($\alpha < 0$). Most experimental β-sheet VCD spectra are complex, yet are typically net negative, which is consistent with a negative α, or right-handed twist of the sheet. Finally we should note that all these computed intensities are quite weak, $\Delta\epsilon/\epsilon$ is of the order of $2–3 \times 10^{-5}$ whereas such values calculated for helices are typically $>10^{-4}$. This is

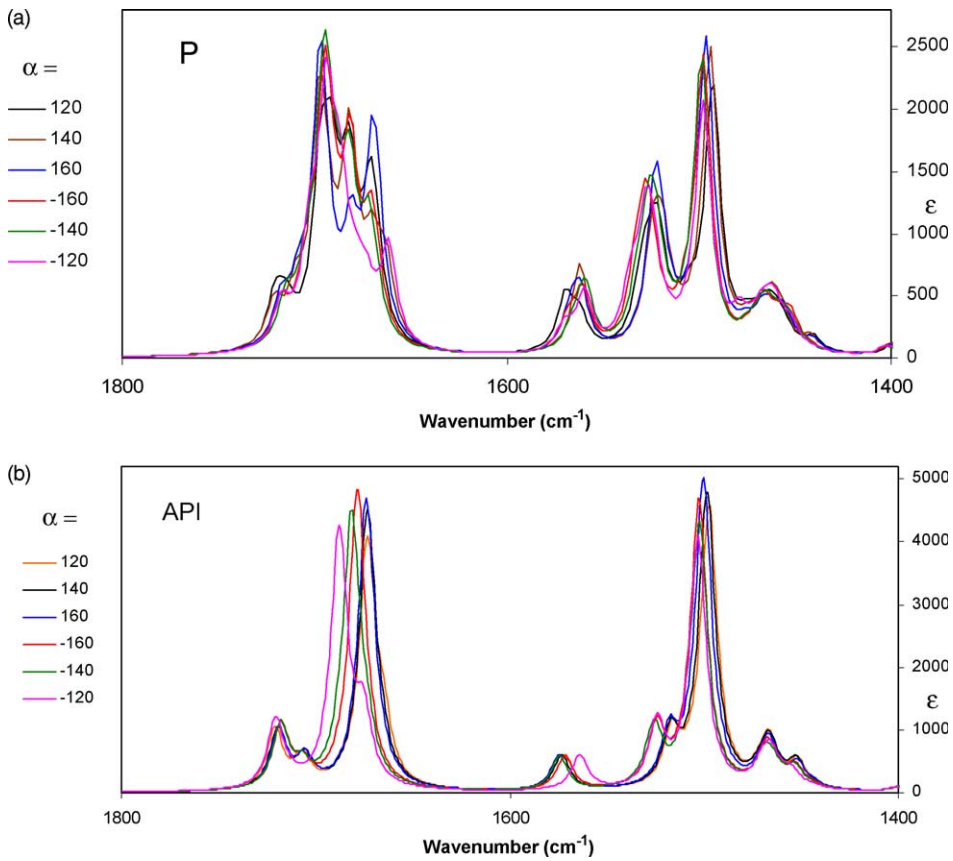

Fig. 6. Simulated IR absorption spectra of six twisted ($\alpha = 120$, 140, 160°, −160, −140 and −120°) parallel (P, top) and anti-parallel (API, bottom) β-sheet models over the amide I and II region.

consistent with the weak VCD found experimentally with β-sheet peptides and proteins.

4. Discussion

4.1. Optimized structures and associated spectra

In this paper we have shown results for optimizing the geometry of a model β-sheet, two strands of four amides each, in parallel and two anti-parallel conformations. All calculations were for peptides in vacuum and were done at a reasonable level using DFT methods. We have gone further and simulated IR and VCD spectra for these structures to see if the computed properties have any relationship with experimental observations. The simulations show qualitative agreement with results for β-sheet peptides and proteins. To our knowledge this is the first complete optimization for a β-sheet structure of this size at the DFT level. The resulting geometry of the anti-parallel form generally reflects expectations based on numerous peptide and protein structures [57]. The ϕ, ψ angles were almost constant for API but showed more variation in APII at the end residues (Table 2). This variance is probably due to the positioning of the interstrand H-bonds closer to the termini for API and the fewer stabilizing outer-edge, H-bonded rings in APII. Nonetheless, all computed angles are well within the expected ϕ, ψ area of the Ramachandran map for β-sheet conformations abstracted from protein structures [58].

The parallel structure is decidedly more distorted than found in model proteins with extended parallel sheets, such as the β-helix or TIM barrel [59,60]. This suggests that adding more strands to this parallel model may have a significant impact on the geometry. If this were the goal, it would have been possible to constrain the calculation to have translational symmetry, so that sheets could be more naturally assembled. At present we do not have capabilities to carry out calculations with more strands, but do plan to explore them in the future. However, results obtained so far [56] indicate that IR and VCD spectra are primarily determined by short-range interactions. Thus these DFT calculations, which are necessarily more limited in size, maintain a useful role for interpreting spectral data. The experimental frequencies, in particular, would be influenced by non-covalent interactions of the amide groups either with solvent or with other polar residues. Comparison of our calculational two-stranded parallel sheet results may be possible with data for model structures now being

Table 3
The dependence of the amide I and amide II absorption maxima (cm^{-1}) on the sheet twist

Twist (α)	Natural						Deuterated					
	P		API		APII		P		API		APII	
	AI	AII	AI	AII	AI	AII	AI	AII	AI	AII	AI	AII
120°	1692	1492	1673	1497	1669	1496	1688	1420	1670	1430	1668	1424
140°	1694	1498	1673	1490	1672	1496	1688	1418	1671	1431	1670	1426
160°	1696	1496	1674	1500			1692	1420	1672	1430		
180°	1696	1497	1676	1501	1675	1505	1690	1422	1675	1432	1673	1423
−160°	1694	1498	1678	1502			1688	1420	1676	1432		
−140°	1694	1498	1681	1502	1680	1508	1688	1418	1678	1430	1676	1406
−120°	1694	1498	1688	1503	1684	1505	1686	1416	1685	1419	1681	1398

synthesized that have parallel strands linked at one end by a mimetic that allows chain reversal at the turn [61,62]. However, in such hairpins with anti-parallel strands and a more normal, peptidic linkage, the twist angles developed are much larger than we calculate for our geometry optimized, model anti-parallel two-strand assembly. Thus to obtain realistic structures with DFT optimization presumably requires some added component. For multi-stranded geometries, the first component to consider is of course the added strands. For a two-stranded assembly, interactions with the solvent and the steric repulsion and variable hydrophobicity of realistic side-chains need to be considered and would probably lead to more twist.

4.2. The impact of twisting

To explore the effect of twisting, we systematically varied the twist angle, re-minimized the other coordinates and then simulated spectral properties for that revised geometry. Though constrained in the overall sense of twist, these calculations were otherwise fully optimized, thus providing a more relaxed model (closer to the potential minimum) than our previous studies of the twisting effect upon spectra [26]. An alternative DFT study of twisting effects on β-structures has appeared that used smaller peptides (one or two amides) for calculational modeling [63]. Those authors concluded that the right-hand twisting propensity was intrinsic to the peptide backbone but only tended to appear when 'unleashed' by interstrand H-bonds. This argument, though consistent with their calculational results, seems to have some logical flaws that may make it less general than the authors postulate. First, single strands that do not H-bond to themselves in 3_{10}-, α-, or π-helices for example, or to other strands, in β-sheets, do actually tend to form left-handed structures. These were often characterized as 'random-coils' but are now widely recognized to share

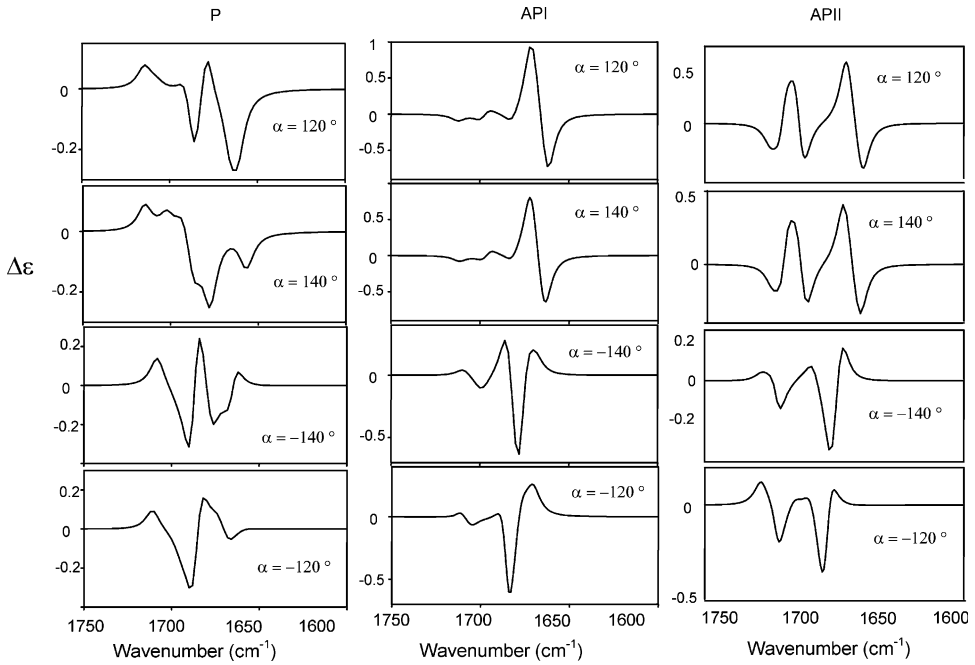

Fig. 7. The simulated amide I′ VCD bandshape dependence on the sheet twist angle ($\alpha = 120$, 140, −140 and −120°) for the N-deuterated P (left), API (center) and APII (right) forms.

the left-handed helicity of the poly-L-proline (P_{II}) structure [24,64]. If somewhat unwound, these left-handed P_{II} strands would indeed H-bond to other strands yielding a sheet with a right-hand twist. This seeming handedness reversal is a natural result of the sheet utilizing every other amide C=O or N–H to form inter-strand H-bonds. If a peptide helix has between 2 and 4 residues per turn, an extended structure based on an every other reside repeat will make a network of opposite handedness to one based sequentially on every residue. This is a simple consequence of geometry. Thus the inherent tendency of the twist can be seen to be apparent in single strands, and should support the assertion of an intrinsic twist propensity [63] but is actually tempered, not released, by interstrand H-bond formation in realistic sheets, since long strands cannot both significantly twist and form a sheet [55]. This is why extended sheet structures such as aggregates are relatively flat.

Our two strand fully minimized results are consistent with this empirical observation in that they yield anti-parallel sheets that are in fact almost flat, with only a slight right hand twist. Thus the interstrand H-bonds actually do not release the inherent tendency in an extended peptide. The difference in our calculation is one of looking at longer, more realistic strands as opposed to the dipeptides used in that earlier study [63]. Our structures show that the adjacent H-bonds have angular variations that are large as compared to the average twist per residue. This bond-to-bond variation becomes much more apparent when the entire structure is constrained to specific twist angles. Finally, one has to realize the intrinsic limits of DFT methods, for example their failure to describe properly the van der Waals interactions [65], especially in modeling of biopolymer secondary structures whose relative stability is dependent on tiny differences ($\sim 10^{-4}$%) in the total molecular energy.

Spectra calculated for this simple two-strand sheet do qualitatively reflect the experimental characteristics of the IR and VCD amide I bands. Comparison to Amide II data is much more difficult due to the lack of solvent in our calculations and its presence (generally as D_2O) in most experimental spectra. These calculations do have relevance to the growing body of experimental data for hairpin structures, which, if stable, have two anti-parallel strands [35,66–70]. The variation in IR and VCD spectra predicted here reflect results obtained with earlier specific geometry constrained calculations [26], but in this paper are computed for relaxed structures. Our previous study implied that twisting would reduce the amide I exciton width and increase its VCD intensity. This study goes further to show the effects to be sensitive to the sign of the twist angle and the sign pattern to be diagnostic of twist type. The intensity distribution over the exciton band varied between parallel and anti-parallel structures in both calculations, but was more pronounced in these fully minimized calculations. In particular, for positive α angles (left hand twist of the sheet) the maximal splitting was calculated for the API geometry, approximately corresponding to the value for the flat sheet. However for negative α values, (right-hand twist) the API exciton splitting decreases sharply and thus the typical IR absorption maximum increases in frequency. For the parallel conformer, the maximum is mid-band, and the lower frequency component loses intensity in going from positive to negative α values.

Whether or not that conformationally dependent intensity variation we have calculated with these model DFT spectral simulations will be useful in practice remains to be seen, since the fully minimized parallel structure, in particular, has more distortion than would be consistent with a multi strand parallel sheet, and both optimized anti-parallel structures have less twist. Nonetheless it is clear that the anti-parallel structure is dominated in the IR by an intensity distribution over the exciton band that places maximal intensity on one of the lower components, that one which has each carbonyl vibration out of phase with its nearest neighbor in the strand, and weights the central, interstrand H-bonded C=O groups the most [27]. The VCD for this intense band is dominated by a negative component that in these calculations appears to part of a negative couplet. In the parallel case IR intensity is more in the band center and the VCD is again primarily negative in that same band center.

5. Conclusion

As experimental data develop for more well-defined structures, the ultimate validity of these predictions of conformationally sensitive spectral patterns will be tested. Similarly, as our computational capabilities increase, longer and more strands can be incorporated in these DFT model calculations. From another point of view, we are already carrying out related calculations using explicit waters to solvate edge amide groups. Incorporating all these aspects into a consistent model will allow much more reliable spectral and structural modeling with DFT methods in the future. Such incorporation is possible using the transfer techniques we have employed for previous, non-fully optimized simulations.

This work was supported by the Grant Agency of the Academy of Sciences (A4055104), Grant Agency of the Czech Republic (grant 203/01/0031), and by grants (to TAK) from the National Science Foundation (CHE 03-16014) and from the donors of the Petroleum Research Fund, administered by the American Chemical Society.

References

[1] S. Krimm, J. Bandekar, Adv. Protein Chem. 38 (1986) 181.
[2] P.J. Stephens, J. Phys. Chem. 89 (1985) 748.
[3] P.J. Stephens, J. Phys. Chem. 91 (1987) 1712.

[4] P.J. Stephens, F.J. Devlin, C.S. Ashvar, C.F. Chabalowski, M.J. Frisch, Faraday Discuss. 99 (1994) 103.
[5] P.J. Stephens, F.J. Devlin, C.F. Chabalowski, M.J. Frisch, J. Phys. Chem. 98 (1994) 11623.
[6] K.L. Bak, F.J. Devlin, C.S. Ashvar, P.R. Taylor, M.J. Frisch, P.J. Stephens, J. Phys. Chem. 99 (1995) 14918.
[7] J.R. Cheeseman, M.J. Frisch, F.J. Devlin, P.J. Stephens, Chem. Phys. Lett. 252 (1996) 211.
[8] P.J. Stephens, C.S. Ashvar, F.J. Devlin, J.R. Cheeseman, M.J. Frisch, Mol. Phys. 89 (1996) 579.
[9] P. Bour, J. Kubelka, T.A. Keiderling, Biopolymers 53 (2000) 380.
[10] P. Bour, J. Kubelka, T.A. Keiderling, Biopolymers 65 (2002) 45.
[11] J. Kubelka, R.A.G.D. Silva, P. Bour, S.M. Decatur, T.A. Keiderling, in: J.M. Hicks (Ed.), Chirality: Physical Chemistry, ACS Symposium Series, vol. 810, American Chemical Society, Washington DC, 2002, p. 50.
[12] J. Kubelka, R.A.G.D. Silva, T.A. Keiderling, J. Am. Chem. Soc. 124 (2002) 5325.
[13] R.A.G.D. Silva, J. Kubelka, S.M. Decatur, P. Bour, T.A. Keiderling, Proc. Natl Acad. Sci. USA 97 (2000) 8318.
[14] K.J. Jalkanen, S. Suhai, Chem. Phys. 208 (1996) 81.
[15] W.-G. Han, K.J. Jalkanen, M. Elstner, S. Suhai, J. Phys. Chem. B 102 (1998) 2587.
[16] M. Knapp-Mohammady, K.J. Jalkanen, F. Nardi, R.C. Wade, S. Suhai, Chem. Phys. 240 (1999) 63.
[17] H.G. Bohr, K.J. Jalkanen, M. Elstner, K. Frimand, S. Suhai, Chem. Phys. 246 (1999) 13.
[18] R. Schweitzer-Stenner, F. Eker, Q. Huang, K. Griebenow, P.A. Mroz, P.M. Kozlowski, J. Phys. Chem. B 106 (2002) 4294.
[19] P. Bour, T.A. Keiderling, J. Am. Chem. Soc. 115 (1993) 9602.
[20] E. Tajkhorshid, K.J. Jalkanen, S. Suhai, J. Phys. Chem. B 102 (1998) 5899.
[21] R. Schweitzer-Stenner, G. Sieler, N.G. Mirkin, S. Krimm, J. Phys. Chem. 102 (1998) 118.
[22] J. Kubelka, T.A. Keiderling, J. Phys. Chem. A 105 (2001) 10922.
[23] P. Bour, J. Sopkova, L. Bednarova, P. Malon, T.A. Keiderling, J. Comput.Chem. 18 (1997) 646.
[24] Z. Shi, R.W. Woody, N.R. Kallenbach, Adv. Prot. Chem. 62 (2002) 163.
[25] G.L. Millhauser, Biochemistry 34 (1995) 3873.
[26] J. Kubelka, T.A. Keiderling, J. Am. Chem. Soc. 123 (2001) 12048.
[27] J. Kubelka, T.A. Keiderling, J. Am. Chem. Soc. 123 (2001) 6142.
[28] J. Hilario, J. Kubelka, F.A. Syud, S.H. Gellman, T.A. Keiderling, Biopolymers (Biospectroscopy) 67 (2002) 233.
[29] S.C. Yasui, T.A. Keiderling, J. Am. Chem. Soc. 108 (1986) 5576.
[30] V. Baumruk, D.F. Huo, R.K. Dukor, T.A. Keiderling, D. Lelievre, A. Brack, Biopolymers 34 (1994) 1115.
[31] T.A. Keiderling, R.A.G.D. Silva, G. Yoder, R. Dukor, K. Bioorg, Med. Chem. 7 (1999) 133.
[32] T.A. Keiderling, in: N. Berova, K. Nakanishi, R.W. Woody (Eds.), Circular Dichroism: Principles and Applications, Wiley, New York, 2000, p. 621.
[33] P. Pancoska, S.C. Yasui, T.A. Keiderling, Biochemistry 30 (1991) 5089.
[34] P. Pancoska, E. Bitto, V. Janota, M. Urbanova, V.P. Gupta, T.A. Keiderling, Protein Sci. 4 (1995) 1384.
[35] S.H. Gellman, Curr. Opin. Struct. Biol. 2 (1998) 717.
[36] R.P. Cheng, S.H. Gellman, W.F. DeGrado, Chem. Rev. 101 (2001) 3219.
[37] J. Venkatraman, S. Shankaramma, P. Balaram, Chem. Rev. 101 (2001) 3131.
[38] M. Searle, JCS-Perkin Trans. II (2001) 1011.
[39] L. Serrano, Adv. Prot. Chem., Vol. Vol 53: Protein Folding Mechanisms., 2000, p. 49.
[40] P. Bour, T.A. Keiderling, J. Chem. Phys. 117 (2002) 4126.
[41] S.A. Asher, A. Ianoul, G. Mix, M.N. Boyden, A. Karnoup, M. Diem, R. Schweitzer-Stenner, J. Am. Chem. Soc. 123 (2001) 11775.
[42] Z.H. Chi, S.A. Asher, Biochemistry 37 (1998) 2865.
[43] G. Sieler, R. Schweitzer-Stenner, J. Holtz, V. Pajcini, S. Asher, J. Phys. Chem. B 103 (1999) 372.
[44] R. Schweitzer-Stenner, J. Raman Spectrosc. 32 (2001) 711.
[45] L.D. Barron, L. Hecht, E.W. Blanch, A.F. Bell, Prog. Biophys. Mol. Biol. 73 (2000) 1.
[46] P. Bour, J. Kubelka, T. A. Keiderling, to be submitted,.
[47] H. Torii, T. Tatsumi, M. Tasumi, J. Raman, J. Raman Spectrosc. 29 (1998) 537.
[48] M. J. Frisch, G. W. Trucks, H. B. Schlegel, G. E. Scuseria, M. A. Robb, J. R. Cheeseman, V. G. Zakrzewski, J. Montgomery, J. A., R. E. Stratmann, J. C. Burant, S. Dapprich, J. M. Millam, A. D. Daniels, K. N. Kudin, M. C. Strain, O. Farkas, J. Tomasi, V. Barone, M. Cossi, R. Cammi, B. Mennucci, C. Pomelli, C. Adamo, S. Clifford, J. Ochterski, G. A. Petersson, P. Y. Ayala, Q. Cui, K. Morokuma, D. K. Malick, A. D. Rabuck, K. Raghavachari, J. B. Foresman, J. Cioslowski, J. V. Ortiz, B. B. Stefanov, G. Liu, A. Liashenko, P. Piskorz, I. Komaromi, R. Gomperts, R. L. Martin, D. J. Fox, T. Keith, M. A. Al-Laham, C. Y. Peng, A. Nanayakkara, C. Gonzalez, M. Challacombe, P. M. W. Gill, B. Johnson, W. Chen, M. W. Wong, J. L. Andres, C. Gonzalez, M. Head-Gordon, E. S. Replogle, J. A. Pople, Gaussian, Inc., Pittsburgh PA, 1998.
[49] C. Peng, P.Y. Ayala, H.B. Schlegel, F.M.J. J, Comp. Chem. 17 (1996) 49.
[50] R.V. Pappu, R.K. Hart, J.W. Ponder, J. Phys. Chem. B 102 (1998) 9725.
[51] P. Bour, J. McCann, H. Wieser, J. Phys. Chem. A 101 (1997) 9783.
[52] P. Bour, J. McCann, H. Wieser, J. Phys. Chem. A 102 (1998) 102.
[53] V. Andrushchenko, H. Wieser, P. Bour, J. Phys. Chem. B 106 (2002) 12623.
[54] M.W. MacArthur, J.M. Thorton, J. Mol. Biol. 264 (1996) 1180.
[55] F.R. Salemme, Prog. Biophys. Mol. Biol. 42 (1983) 95.
[56] J. Kubelka, PhD Thesis, University of Illinois at Chicago, Chicago, 2002.
[57] T.E. Creighton, Proteins: Structures and Molecular Properties, W.H. Freeman and Co, New York, 1993.
[58] J.M. Thornton, in: T.E. Creighton (Ed.), Protein Folding, W.H. Freeman, New York, 1992, p. 59.
[59] M.D. Yoder, F. Jurnak, Plant. Physiol. 107 (1995) 349.
[60] C. Branden, J. Tooze, Introduction to Protein Structure, Garland Publishing, New York, 1998.
[61] P. Chitnumsub, W.R. Fiori, H.A. Lashuel, H. Diaz, J.W. Kelly, Bioorg. Med. Chem. 7 (1999) 39.
[62] M.G. Woll, J.R. Lai, I.A. Guzei, S.J.C. Taylor, M.E.B. Smith, S.H. Gellman, J. Am. Chem. Soc. 123 (2001) 11077.
[63] I.L. Shamovsky, G.M. Ross, R.J. Riopelle, J. Phys. Chem. B 104 (2000) 11296.
[64] R.K. Dukor, T.A. Keiderling, Biopolymers 31 (1991) 1747.
[65] N. Kurita, H. Inoue, H. Sekino, Chem. Phys. Lett. 370 (2003) 161.
[66] C. Zhao, P.L. Polavarapu, C. Das, P. Balaram, J. Am. Chem. Soc. 122 (2000) 8228.
[67] J. Venkatraman, S.C. Shankaramma, P. Balaram, Chem. Rev. 101 (2001) 3131.
[68] M. Ramirez-Alvarado, T. Kortemme, F.J. Blanco, L. Serrano, Bioorg. Med. Chem. 7 (1999) 93.
[69] E. Lacroix, T. Kortemme, M. Lopez de la Paz, L. Serrano, Curr. Opp. Struct. Biol. 9 (1999) 487.
[70] C.L. Nesloney, J.W. Kelly, Bioorg. Med. Chem. 4 (1996) 739.
[71] R.D.B. Fraser, T.P. McRae, Conformation in Fibrous Proteins, Academic Press, New York, 1973.
[72] G. Scapin, J.I. Gordon, J.C. Sacchettini, J. Biol. Chem. 267 (1992) 4253.